TITLE:

Ultrahigh-Q nanocavities in two-dimensional photonic crystal slabs

AUTHOR(S):

Asano, T; Song, BS; Akahane, Y; Noda, S

CITATION:

Asano, T ...[et al]. Ultrahigh-Q nanocavities in two-dimensional photonic crystal slabs. IEEE JOURNAL OF SELECTED TOPICS IN QUANTUM ELECTRONICS 2006, 12(6): 1123-1134

ISSUE DATE:
2006

URL:
http://hdl.handle.net/2433/50166

RIGHT:
(c)2006 IEEE. Personal use of this material is permitted. However, permission to reprint/republish this material for advertising or promotional purposes or for creating new collective works for resale or redistribution to servers or lists, or to reuse any copyrighted component of this work in other works must be obtained from the IEEE.

京都大学学術情報リポジトリ
KURENAI 紅
Kyoto University Research Information Repository

京都大学 KYOTO UNIVERSITY
A Self-archived copy in
Kyoto University Research Information Repository
https://repository.kulib.kyoto-u.ac.jp
京都大学学術情報リポジトリ KURENAI 紅 Kyoto University Research Information Repository

IEEE JOURNAL OF SELECTED TOPICS IN QUANTUM ELECTRONICS, VOL. 12, NO. 6, NOVEMBER/DECEMBER 2006

Ultrahigh-Q Nanocavities in Two-Dimensional Photonic Crystal Slabs

Takashi Asano, Bong-Shik Song, Yoshihiro Akahane, and Susumu Noda, *Member, IEEE*

(Invited Paper)

***Abstract*—In this paper, we discuss methods to suppress the radiation loss of ultrasmall cavities, of the size of the optical wavelength, in two-dimensional photonic crystal slabs. An important design concept to suppress radiation loss is introduced: The envelope of the cavity mode field should have no abrupt changes and should ideally follow a Gaussian function. Cubic wavelength order cavities, with experimental Q factors of 100 000 and nearly 1 000 000 are obtained by tailoring the envelope functions using air-hole shifts and multistep heterostructures, respectively. In addition, the experimental Q factors of the latest cavities are shown to be determined by the imperfections in the fabricated structures and not by the cavity design. The differences between the experimental and the theoretical Q factors are investigated in order to demonstrate how higher Q factors could be realized in the future.**

***Index Terms*—Heterostructure, photonic crystal slab, radiation loss, ultrasmall optical cavity.**

I. INTRODUCTION

ULTRASMALL cavities that can confine light strongly (high-Q photonic nanocavities) are important in a variety of areas of science and engineering. They are required for the realization of ultrasmall filters with high resolution [1]–[4], ultrasmall sensors [5], low-threshold lasers [6], single-photon emitters [7], compact optical-buffer memories [8], [9], and in the field of quantum computation. For such applications, it is especially important to realize cavities that have both high Q factors and very small modal volumes V because: 1) a large Q factor means a long lifetime of captured photons; 2) a small cavity size ensures single-mode operation for a broad range of wavelengths; 3) a small cavity size enables large-scale integration; and 4) Q/V determines the strength of the interaction between the light and the matter in a cavity. Therefore, there is a growing interest in high-Q photonic nanocavities [10]–[15].

Recently, we reported an important design concept for the realization of high-Q nanocavities in two-dimensional (2-D) photonic crystal (PC) slabs: To suppress radiation loss, the envelope of the cavity mode field should have no abrupt changes and should ideally follow a Gaussian function [16]. We utilized local changes of the photonic bandgap (PBG) effect due to the shift in air-hole positions in order to tailor the envelope functions to be similar to Gaussian functions. A cubic wavelength order cavity, with very high Q factors of 45 000 (experimental) and 100 000 (theoretical), has been developed by this method [16]. Variations of this method have been widely investigated, but in all cases there remain small deviations of the envelope functions from Gaussian functions, which limit the experimental and theoretical Q factors to $<$100 000 and $<$260 000, respectively [17]. To overcome this limitation, we designed a cavity structure based on the novel concept of a photonic double heterostructure, which enabled nearly perfect control of the envelope function of the cavity mode electric field [18]. An experimental Q factor of 600 000 and a theoretical Q factor of 20 000 000 have been demonstrated in this type of cavity [18]. Guidelines toward achieving further increases in Q factor have also been suggested [18].

An inverse approach to the problem, where a cavity structure is calculated from the required envelope function under some level of approximation, has recently been reported by Englund *et al.* [19] . This approach is interesting and useful for the design of cavities with special envelope functions. They succeeded in designing a Gaussian envelope cavity [16], which has a Q factor of nearly theoretical limit. One of the weaknesses of this approach might be the fact that the structures are automatically calculated out of consideration of fabrication technique. It might limit the experimental Q factors of actually fabricated cavities.

In this paper, we explain our concept in detail and show that it is straightforward to achieve high-Q cavities. We describe the design and characteristics of the cavities that we have developed, including a cavity structure with an experimental Q factor of 0.8–1.0 million. In addition, the differences between the experimental and the theoretical Q factors are investigated in order to demonstrate how higher Q factors could be realized in the future.

II. PRINCIPLE OF THE ENVELOPE FUNCTION APPROACH

The Q factor of a resonant mode of a cavity represents the optical energy stored in the cavity over the energy loss per cycle of the light. When the material of the cavity shows no absorption, the energy loss is determined by the radiation loss from the surface of the cavity, while the energy stored in the cavity is proportional to the volume of the cavity, assuming the energy

---

Manuscript received March 1, 2006; revised June 19, 2006. This work was supported in part by the Ministry of Education, Culture, Sports, Science and Technology of Japan under a Grant-in-Aid and also in part by Core Research for Evolutional Science and Technology of the Japan Science and Technology Agency.

T. Asano and S. Noda are with the Department of Electronic Science and Engineering, Kyoto University, Kyoto 615-8510, Japan (e-mail: tasano@kuee.kyoto-u.ac.jp; snoda@kuee.kyoto-u.ac.jp).

B.-S. Song was with Kyoto University, Kyoto 615-8510, Japan. He is now with the School of Information and Communication Engineering, Sungkyunkwan University, Suwon, Korea (e-mail: songwiz@skku.edu).

Y. Akahane was with Kyoto University, Kyoto 615-8510, Japan. He is now with Sumitomo Electric Works, Osaka 571-8686, Japan (e-mail: y-akahane@sei.co.jp).

Digital Object Identifier 10.1109/JSTQE.2006.881639

1077-260X/$20.00 © 2006 IEEE

A Self-archived copy in
Kyoto University Research Information Repository
https://repository.kulib.kyoto-u.ac.jp

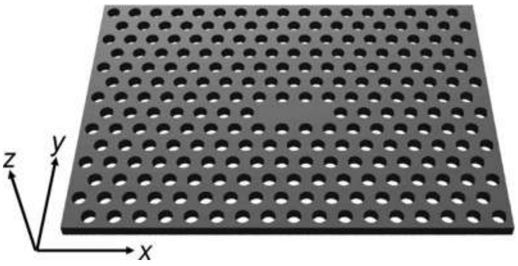

Fig. 1. Photonic nanocavity using a defect in a 2-D PC slab.

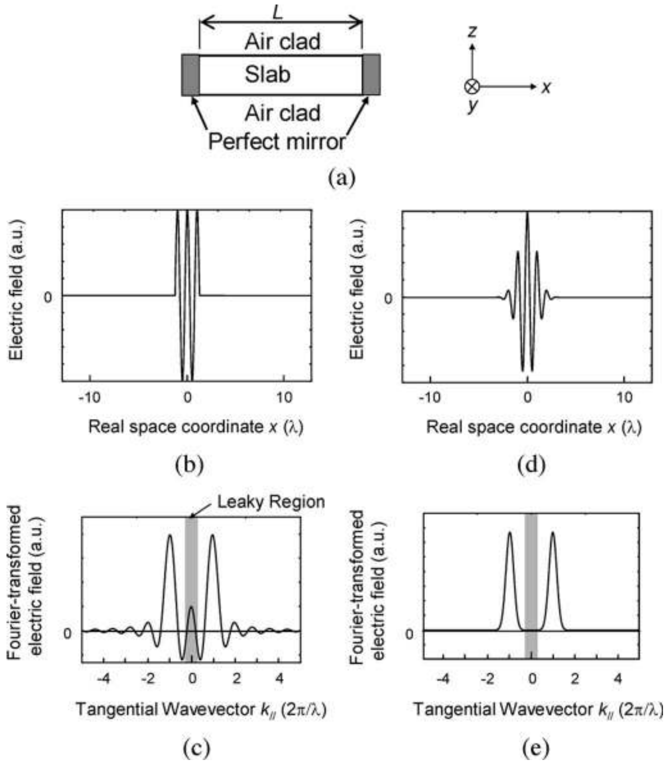

Fig. 2. Analysis of cavities with different inplane confinement. (a) Simplified model of a cavity. (b) Electric field profile of a cavity with a rectangular envelope function, and (c) its spatial FT spectrum. (d) The electric field profile of a cavity with a Gaussian envelope function, and (e) its spatial FT spectrum.

density is constant. The Q factor of a cavity generally decreases with the cavity size, as the ratio of the surface area to the volume increases. The suppression of the radiation loss is crucial to the realization of high-Q nanocavities. One of the most promising solutions is the use of photonic crystals (PCs), which are structures containing periodic changes of the dielectric constant in two or three dimensions. The repeat distances are of the order of the wavelength of light. In a three-dimensional (3-D) PC, there might be a frequency range where no propagating light modes exist in any direction, called a PBG. A small void, or dielectric volume, surrounded by such a 3-D PC [20] would become the ultimate photonic nanocavity with an ultralarge Q/V ratio. However, at present, fabrication techniques are not sufficiently advanced to make 3-D PCs of sufficient size for the required strong confinement of light (PBG effect). The use of a 2-D PC is considered to be a feasible alternative. A cavity surrounded by a 2-D PC slab with a thickness of the order of the wavelength, as shown in Fig. 1, is a very attractive prospect, due to its capacity to strongly confine light and the availability of fabrication process techniques developed for semiconductor devices. It is relatively easy to fabricate 2-D PCs of a sufficient size to perfectly confine light in both the inplane directions, but the 2-D PBG has no effect on light propagating in the direction normal to the slab plane. Instead, light can be confined in this direction by the total internal reflection (TIR) at the interface between the slab and the cladding layer, if the incident angle is larger than the critical angle. The key to the suppression of the radiation loss is establishing how to fulfill the TIR condition.

To investigate light confinement in a 2-D PC slab cavity more concretely, we introduced a simple model shown in Fig. 2(a), whose structure is assumed to be uniform in the direction normal to the paper. Although the model represents a cavity in 2-D (rather than 3-D) space, the results obtained here can also be applied to real cavities in 2-D PC slabs. The model cavity consists of a dielectric material with a finite thickness and length; perfect mirrors enclose both sides of the cavity. Here, "perfect mirror" is defined as a mirror that has no absorption loss and *no transmission*. We considered two extreme cavities having almost the same size and the same resonant wavelength, but different inplane confinement. One cavity is confined by sharp reflection at the cavity edges, where the mode electric field profile is assumed to have a rectangular envelope function [Fig. 2(b)]. The other is a cavity confined by a spatially distributed reflection, where the mode electric field profile is assumed to have a Gaussian envelope function [Fig. 2(d)]. The electric field profiles shown here are those along the interfaces between the slabs and the cladding (air) of the cavities, but they are similar for all z positions inside each cavity. The real space coordinate is represented by the unit of the wavelength of the resonant mode inside the cavity (λ). Fig. 2(c) and (e) shows the spatial Fourier transformation (FT) spectra of each electric field profile, which represents the plane wave components of the cavity mode. The horizontal axis corresponds to the wavevector tangential to the interface ($k_{//}$). The wavevector of the light in the cladding is k_0; only plane wave components with $|k_{//}|>k_0$ can be confined by the TIR. The gray regions in Fig. 2(c) and (e) represent the region where $|k_{//}|<k_0$, the "leaky region," where the plane wave components of a cavity mode are radiated into the cladding. As can be seen clearly in the figures, the cavity with the rectangular envelope [Fig. 2(b) and (c)] has a cavity mode with a greater component inside the leaky region, compared to the cavity with the Gaussian envelope [Fig. 2(d) and (e)].

An understanding of the difference between the two cavity modes is considered to be key to the realization of high-Q photonic nanocavities. We analyzed the mode electric field profiles by separating them into two functions: A fundamental sinusoidal wave with a wavelength of λ, and an envelope function. A mode electric field profile is expressed as the product of the fundamental wave and the envelope function in real space, while the FT spectrum of a mode electric field profile is expressed as a convolution of the FT spectra of the fundamental wave and the envelope function. The FT of the fundamental wave gives

京都大学 KYOTO UNIVERSITY
A Self-archived copy in
Kyoto University Research Information Repository
https://repository.kulib.kyoto-u.ac.jp
京都大学学術情報リポジトリ KURENAI 紅
Kyoto University Research Information Repository

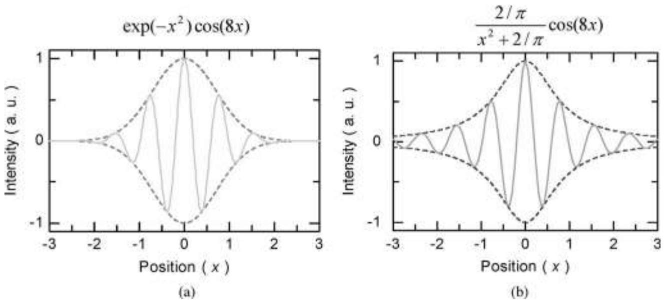

Fig. 3. Examples of cavity fields with (a) Gaussian and (b) Lorentzian envelope functions. Here, the parameters are set in order to make the mode volume of the two cavities equal to one another.

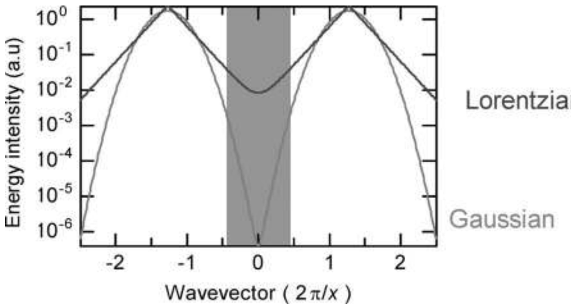

Fig. 4. Energy profiles in Fourier space for the (a) Gaussian and (b) Lorentzian cavity fields in Fig. 3.

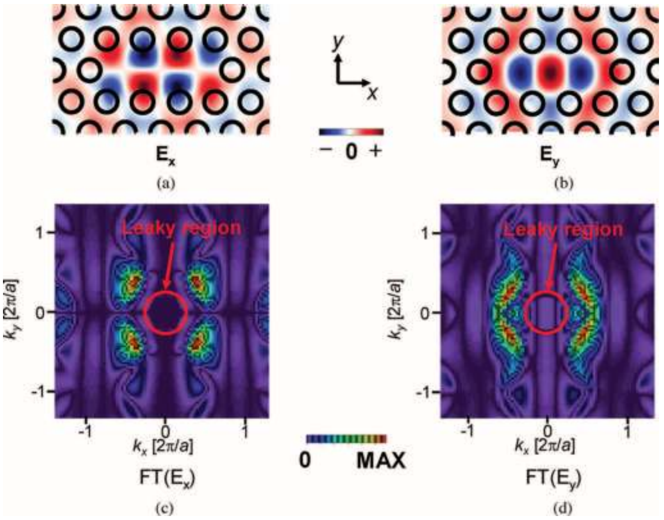

Fig. 5. (a) E_x and (b) E_y electric field profiles of the fundamental resonant mode of the cavity formed by the omission of three air holes, respectively. (c), (d) 2-D Fourier transform spectra of E_x and E_y electric field profiles, respectively. The leaky regions are indicated by *red circles*.

two delta functions at $k_{//} = \pm 2\pi/\lambda$, and the FT of the envelope gives a function with finite width, according to the shape in real space. Since the FT of the fundamental wave is outside the leaky region, it is clear that the components within the leaky region are generated by the convolution with the envelope spectra. The convolution of the fundamental delta function and the envelope spectrum is equal to the sum of two envelope spectra, shifted by $+2\pi/\lambda$ and $-2\pi/\lambda$, respectively. Therefore, the higher spatial frequency components of the envelope spectrum, with $2\pi/\lambda - k_0 < |k_{//}| < 2\pi/\lambda + k_0$, are transferred to the leaky region. The FT mode electric field associated with the rectangular envelope function [Fig. 2(b) and (c)] has a large component in the higher spatial frequency region, due to the abrupt changes in the envelope function at both edges, giving large radiation losses. In contrast, the mode electric field profile associated with the Gaussian envelope function [Fig. 2(d) and (e)] has only a small component in the higher spatial frequency region, due to the smooth variation of the envelope function in real space, giving small radiation losses. It is clear that the shape of the envelope function has a critical effect on the radiation loss of the model cavity, and that, to obtain high-Q factors, abrupt changes in the envelope function should be avoided. However, the confinement of light to regions with dimensions of the order of optical wavelengths requires a spatially localized envelope function of the same dimensions. In order to realize a high-Q photonic nanocavity, the envelope function should not have high-frequency components but should remain spatially localized. As shown here, a Gaussian function can fulfill both these conditions.

We investigated several functions, which were both gently varying and spatially localized, in order to check which function was most appropriate for high photonic nanocavities. Here, as an example, we compare the Lorentzian and the Gaussian envelopes. Fig. 3(a) and (b) shows the cavity field profiles with Gaussian and Lorentzian envelopes, respectively. The parameters of the envelopes were chosen such that the modal volumes of the cavities were equal. Fig. 4 shows the Fourier transformations of the cavity fields. We see that the fraction of the Gaussian envelope cavity mode in the leaky region is much smaller than that of the Lorentzian envelope cavity mode. Although the full-width at half-maximum (FWHM) of the FT spectrum of the Lorentzian function is smaller than that of the Gaussian function, the higher frequency components are opposite, as can be seen in Fig. 4. An exponential envelope function was also investigated. Theoretically, a sinc function is considered to be the best for suppressing radiation loss because the FT spectrum is rectangular, however, it is considered difficult to precisely form an envelope function of such a complex shape in reality. Therefore, at this moment, we believe that the Gaussian envelope is the most appropriate and feasible envelope for confining light in a 2-D PC slab cavity.

III. AIR-HOLE SHIFT CAVITY

A. Design

On the basis of the above considerations, we designed a high-Q photonic nanocavity in a 2-D PC slab (see Fig. 1). The basic structure was silicon with a triangular-lattice pattern of air rods, with a lattice constant of a. The cavity was created by the omission of three air rods in a line along the Γ–J direction (Fig. 1) [21], [22]. The thickness of the slab and the radius of the air rods were $0.6a$ and $0.29a$, respectively. The electric field profiles, E_x and E_y, of the fundamental mode of the cavity were calculated using a 3-D finite-difference time-domain (FDTD) method, and are shown in Fig. 5(a) and (b), respectively. The refractive index of the slab, n, was assumed

京都大学 KYOTO UNIVERSITY
A Self-archived copy in
Kyoto University Research Information Repository
https://repository.kulib.kyoto-u.ac.jp
京都大学学術情報リポジトリ KURENAI 紅 Kyoto University Research Information Repository

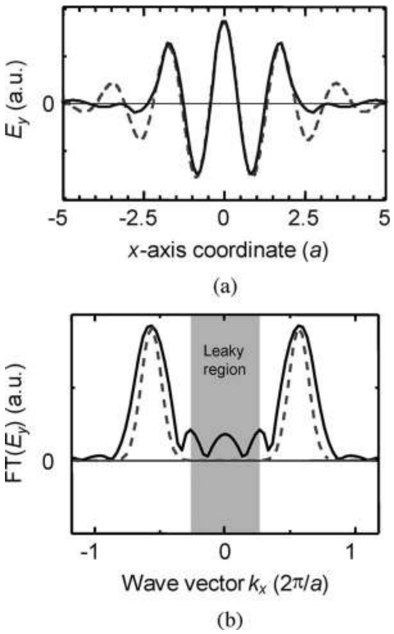

(a)

(b)

Fig. 6. (a) E_y electric field profile along the centerline along the x direction of the cavity, shown in Fig. 5 (*solid line*); a fitting curve obtained by using the same fundamental wave and Gaussian envelope function (*broken line*). (b) FT spectra of the E_y profile (*solid line*) and fitting curve (*broken line*).

to be 3.4. Unlike the models discussed in Section II, the 2-D spatial FT spectra of both E_x and E_y are needed to investigate the vertical confinement [Fig. 5(c) and (d)]. The leaky regions correspond to the region inside the circles with a diameter of k_0 [indicated by red circles in Fig. 5(c) and (d)]. It is seen that the FT spectrum of E_y contains considerable components inside the leaky region, while that of E_x contains little inside the leaky region. The results indicate that to reduce the radiation loss, we should reduce the components of E_y inside the leaky region. E_x has few components inside the leaky region as the E_x field pattern in real space is antisymmetric about the centerline of the cavity along both the x and y directions, as seen in Fig. 5(a), leading to the cancellation of light in the far field. Although at first sight this cancellation mechanism appears an attractive method to suppress radiation loss, it is in fact difficult to obtain ultrahigh-Q nanocavities using this cancellation effect based on symmetry alone. We will not go into further detail here, since this cancellation mechanism has been discussed previously in many papers [10], [13], [14], [22].

Now let us concentrate on E_y. As discussed before, the components in the leaky region of the FT spectrum of E_y are considered to be generated by abrupt changes of the envelope function. To simplify the evaluation, we focused on the E_y profile along the centerline of the cavity along the x direction in real space [solid line in Fig. 6(a)]. We chose this profile because the electric field is concentrated here and resembles that of a one-dimensional cavity resonating along the centerline. In order to evaluate where and what kind of abrupt changes the envelope has, we fitted the envelope with a Gaussian function, which we have shown is ideal for the realization of high-Q nanocavities. In practice, we fitted the E_y profile with a curve generated from a sinusoidal wave with the same wavelength as the fundamental wave of the E_y profile and a Gaussian function [broken line in Fig. 6(a)]. The fitting curve agrees well with the E_y profile around the center of the cavity, but at the edges of the cavity, the envelope of the E_y profile decreases more abruptly than the Gaussian function. The FT spectra of both the E_y profile and the fitting curve were calculated and are shown in Fig. 6(b). As can be seen in the figure, the former has a large component in the leaky region, while the latter does not. It is clear that the origin of the components in the leaky region is the difference between the E_y profile and the fitting curve at the cavity edges. The abrupt decrease of the envelope of the E_y profile at the cavity edge is considered to generate high spatial frequency components in the Fourier space, which are transferred to the leaky region by convolution with the fundamental delta functions, as discussed earlier. Therefore, this abrupt change of the envelope of the E_y profile at the cavity edge must be reduced in order to increase the cavity Q factor.

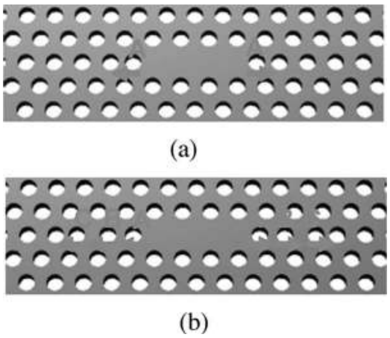

(a)

(b)

Fig. 7. (a) Designed cavity structure created by displacing two air holes at both the edges in order to obtain a high-Q factor. (b) Designed cavity structure created by fine tuning the positions of six air holes near both the edges to obtain an even higher Q factor.

For this purpose, the air-hole positions at the cavity edges were adjusted to lie slightly outside the cavity, as shown in Fig. 7(a). By this adjustment, reflections at the cavity edge are expected to be weakened, as the periodicity of the air holes is disturbed: therefore, the PBG effect is expected to be weakened. The electric field distribution calculated for a cavity structure with an air-hole displacement of $0.20a$ is shown in Fig. 8(a); the electric field profile along the centerline (along the x direction) is shown in Fig. 8(b) together with the fitting curve, generated as described above. As shown in Fig. 8(b), the electric field profile of the adjusted cavity is more similar to the fitting curve than that of the original cavity without air-hole displacement. The FT spectra of the electric field profile of the cavity and the fitting curve are shown in Fig. 8(c). As can be clearly seen in this figure, the component in the leaky region is dramatically reduced in comparison with that of the original cavity shown in Fig. 5.

Next, the Q factors of the cavities were calculated with varying displacement of the air holes at position A (see Fig. 7) from 0.0a to $0.3a$; the Q factors are evaluated from the decay time of the energy stored in the cavity. The results are shown in Fig. 9(a), together with the modal volumes V, evaluated by the following

京都大学 KYOTO UNIVERSITY
A Self-archived copy in
Kyoto University Research Information Repository
https://repository.kulib.kyoto-u.ac.jp
京都大学学術情報リポジトリ KURENAI 紅
Kyoto University Research Information Repository

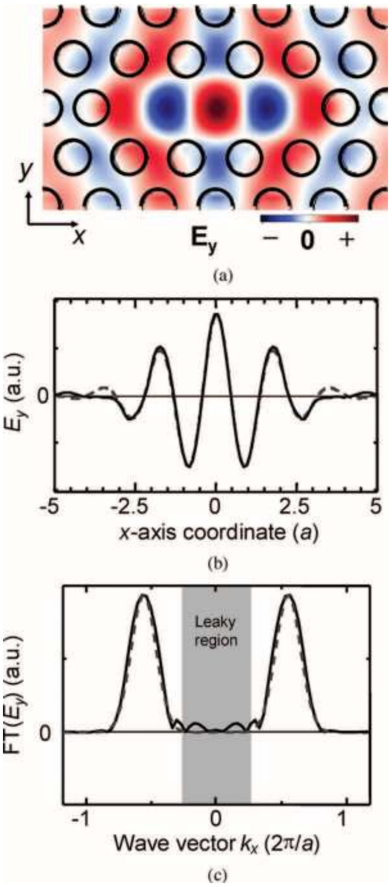

Fig. 8. (a) Electric field (E_y) of the cavity with air-hole displacement of 0.2 a. (b) E_y electric field profile along the centerline of the cavity (*solid line*) and a fitting curve obtained by using the same fundamental wave and Gaussian envelope function (*broken line*). (c) FT spectra of the E_y profile (*solid line*) and the fitting curve (*broken line*).

equation [17]:

$$V = \frac{\int \varepsilon(r)|E(r)|^2 d^3r}{\max[\varepsilon(r)|E(r)|^2]} \tag{1}$$

where $\varepsilon(r)$ is the dielectric constant and $E(r)$ is the electric field.

As seen in the figure, the Q factor increases from 5000 to 100 000 by displacement of the air holes from zero up to $\sim 0.2a$, while the modal volume remains almost constant. This result clearly indicates that the displacement of the air holes is a promising method to increase the Q factor, as expected from the analysis of the electric field profile. The reason that the Q factor decreases for displacements $>0.2a$ can be explained as follows: When the displacement is $>0.2a$, the local decay of the envelope function around $|x| = 2.5a$ becomes smaller than that required to fit the Gaussian function. As a result, the amplitude of the envelope decreases more slowly than the Gaussian function up to $|x| = \sim 2.5a$, and then decays more rapidly outside the shifted holes. The rapid decrease of the envelope function creates higher frequency components in the Fourier space, which lead to reduction of the Q factor. It can be said that fitting the envelope to a Gaussian function is important to obtain high-Q factors.

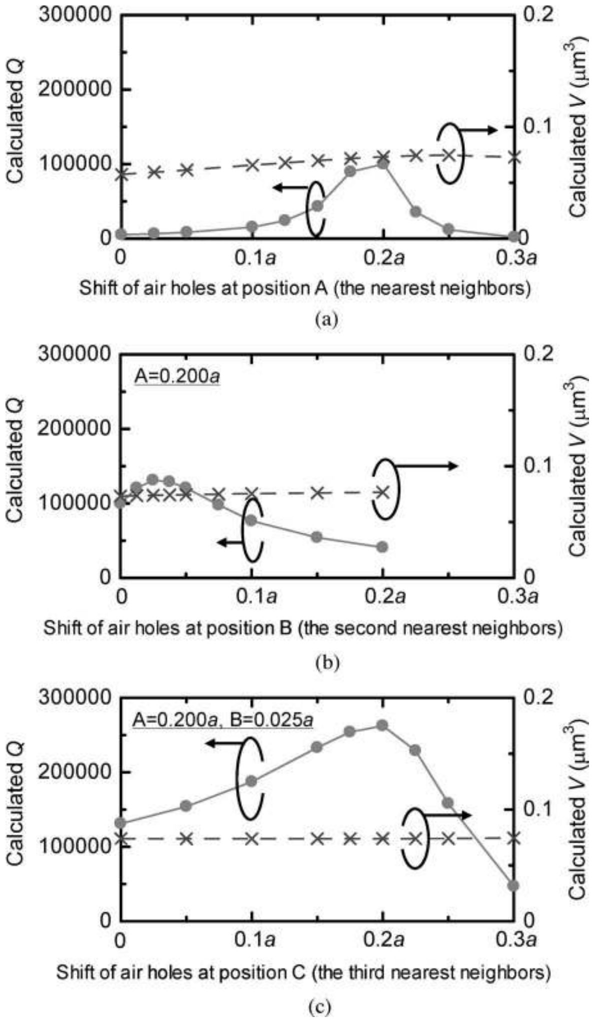

Fig. 9. (a) Cavity Q factors and modal volumes V, obtained theoretically for cavities with a range of displacements of air holes at position A (the nearest neighbors). (b) Those for cavities with a range of displacements of air holes at position B (the second nearest neighbors), while fixing the position of air-holes A at the optimum value of $0.200a$. (c) Those for the cavities with a range of displacements of air holes at position C (the third nearest neighbors), while fixing the positions of air-holes A and B at their optimum values of $0.200a$ and $0.025a$, respectively.

A closer examination of the two curves in Fig. 8(b) shows that, even with an air-hole displacement of $0.20a$, some discrepancy between the modal profile and the fitted curve exists in the region $|x| > 2.5a$. A reduction in this discrepancy is expected to further increase the Q factor of the cavity. We therefore displaced the air holes at position B (the second nearest neighbors, $|x| = 3a$) as shown in Fig. 7(b), while fixing the air holes at position A at an optimum displacement of $0.200a$. The resulting calculated Q factors and the modal volumes are shown in Fig. 9(b). The maximum Q factor, $\sim 130\,000$, was obtained for a displacement of air holes B of $0.025a$. We then shifted the air holes at position C (the third nearest neighbors, $|x| = 4a$), while fixing the positions of air holes A and B at their optimum values. The results are shown in Fig. 9(c). The maximum Q factor, $\sim 260\,000$, was obtained for a displacement of air holes C of $0.200a$. The maximum Q factor calculated here was 50 times larger than that of the cavity without displaced air

A Self-archived copy in
Kyoto University Research Information Repository
https://repository.kulib.kyoto-u.ac.jp

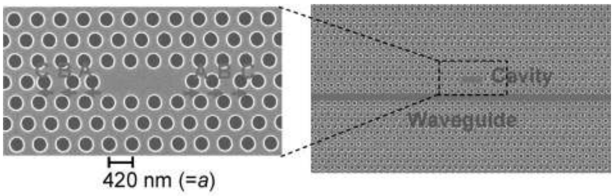

(a) (b)

Fig. 10. SEM images of one of the fabricated samples, including the point-defect cavity with displaced air-holes A, B, and C. (a) Magnified view of the point-defect cavity. (b) Top view of the sample. A line-defect waveguide was introduced near the point-defect cavity.

holes ($Q \sim 5200$). Fig. 9 shows that calculated modal volumes were almost constant with varying air-hole displacements. The modal volume corresponding to the maximum Q factor was $V = 7.4 \times 10^{-14}\mathrm{cm}^3[=0.73(\lambda_0/n)^3]$.

B. Experimental

In order to practically test these theoretical results, we fabricated samples having various air-hole displacements. Initially, a silicon-on-insulator substrate was coated with a resist mask (ZEP-520). PC patterns were drawn on this resist mask by electron-beam lithography. The resist patterns were then transferred to the upper silicon layer using inductively-coupled plasma reactive-ion etching. After the dry-etching procedure, the resist was removed using an O_2 plasma. Finally, the SiO_2 layer under the PC layer was selectively etched away using hydrofluoric acid, to form an air-bridge structure. We selected a lattice constant a of 420 nm and used the same parameters as for the calculated structure described earlier. The PC area was $15 \times 250 \mu\mathrm{m}$. Scanning electron microscope (SEM) images of one of the fabricated samples, including the point-defect cavity with displacement of air holes A, B, and C, are shown in Fig. 10(a) and (b). A line-defect waveguide was also introduced near the point-defect cavity, as shown in Fig. 10(b).

Photons were injected from a line-defect waveguide facet, and the cavities were excited via the waveguide. Light emitted from the cavity into the free space, and that transmitted through the waveguide, was observed. Transmission and radiation spectra are shown in Fig. 11(a) and (b), respectively. From both the spectra, it was possible to evaluate the cavity Q factor experimentally. It is important to note that the Q factor obtained from the line width of the radiation spectrum shown in Fig. 5(b) is the Q factor loaded by the excitation waveguide (Q_{loaded}). The intrinsic Q factor, denoted Q_{exp}, is determined by the coupling loss to free space only. From coupled mode theory Q_{exp} can be expressed as

$$Q_{\mathrm{exp}} = Q_{\mathrm{loaded}}/\sqrt{T} \tag{2}$$

where T is the transmittance at the resonant wavelength of the cavity [17]. The transmittance T is defined as the ratio of the transmitted energy in the presence of the cavity, to the transmitted energy in the absence of the cavity. Experimentally, we can evaluate T as T_2/T_1 [as shown in Fig. 11(a)].

First, we investigated samples with displaced air holes at position A, and evaluated Q_{exp} using the method described earlier. The results are shown in Fig. 12(a). For each fixed air-hole displacement, we measured several samples with line defect waveguides at different distances from the point-defect cavity. The measurements clearly demonstrate good reproducibility. As the air-hole displacements were increased from zero to $0.3a$, Q_{exp} increased drastically and then decreased, in agreement with an earlier work [16]. A maximum value of Q_{exp} of 63 000 was obtained for a displacement of air holes A of $0.176a$. A comparison with the calculated results [Fig. 3(a)] indicates that the theoretical and experimental results were qualitatively similar in terms of variation of Q_{exp} as a function of air-hole displacement. The experimental values were lower than the theoretical ones, for reasons that are discussed in Section V, later.

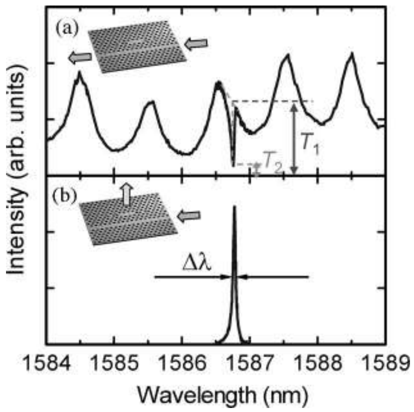

Fig. 11. Examples of the measured spectra of a cavity with displaced air holes. (a) Transmission spectrum and (b) radiation spectrum. The insets in the figures show the geometry of the measured photon fluxes.

Next, we displaced the air holes at position B while fixing the positions of air holes A at the optimum value of $0.176a$. Q_{exp} values are shown in Fig. 12(b). The maximum value of $Q_{\mathrm{exp}} \sim 65\,000$ was obtained for a small shift of air holes B. Finally, we displaced air holes at position C while fixing positions of air holes A and B at their optimum values, and measured the Q factor of the cavities. The results presented in Fig. 12(c) show that a maximum value of Q_{exp} $(\sim 100\,000)$ was obtained for an air-hole C displacement of $0.176a$. Q_{exp} was 20 times larger than that of a cavity with no air-hole displacement ($Q_{\mathrm{exp}} \sim 5000$). These experimental results indicate that displacing the air holes at positions A, B, and C is an effective method for significantly increasing cavity Q factors. The experimental results shown in Fig. 12 and the theoretical results presented in Fig. 9 are qualitatively very similar in terms of the variation of Q_{exp} as a function of displacement of not only the air-holes A, but also displacements of the air-holes B and C.

IV. DOUBLE HETEROSTRUCTURE CAVITY

The results described in Section III clearly demonstrate that the design concept of the envelope function tuning is very effective. However, the strategy for the adjustment of air-hole positions is not very clear when multiple air holes are shifted: Further increases in the Q factor seem to be difficult to obtain. The relationship between the changes in the structure and those

京都大学 KYOTO UNIVERSITY
A Self-archived copy in
Kyoto University Research Information Repository
https://repository.kulib.kyoto-u.ac.jp
京都大学学術情報リポジトリ KURENAI 紅
Kyoto University Research Information Repository

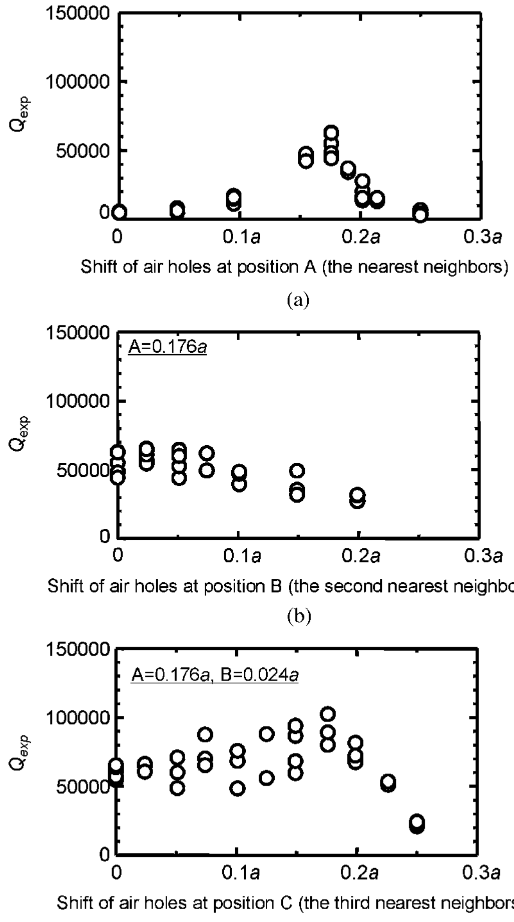

(a)

(b)

(c)

Fig. 12. (a) Cavity Q factors (Q_{V}) obtained experimentally for cavities with various displacements of air holes at position A. (b) Those for cavities with various displacements of air holes at position B, while fixing the position of air-holes A at the optimum value of $0.176a$. (c) Those for the cavities with various displacements of air holes at position C, while fixing the positions of air-holes A and B at their optimum values of $0.176a$ and $0.024a$, respectively.

in the electric profile becomes very complex: for example, a shift of the position of an air hole increases the distance to the neighboring air hole on one side and decreases the separation on the other side. Also, a change of the distance of the air holes induces both a local shift of the PBG central frequency and a local change of the PBG width. A more comprehensive and straightforward method to tune the envelope function of the cavity is required to increase the Q factor further. For this purpose, we proposed the concept of "photonic double-heterostructures" [18], described later.

The basic PC structure used in the construction of the photonic double heterostructure is shown in Fig. 13(a): It is a 2-D PC slab with a triangular-lattice structure and a line-defect waveguide formed by a missing row of air holes in the Γ–J direction. The band diagram of the structure is presented in Fig. 13(b) and shows that the lower frequency edge of the waveguide mode exists within the PBG frequency range. The frequencies above this edge lie within the transmission region, in which propagation modes exist in the waveguide, while the frequencies below this edge lie within the mode-gap region where propagation modes do not exist but evanescent modes can be excited [18]. Two PCs (I and II) were joined to form a double heterostructure [Fig. 13(c)], where the lattice constant of PC I (a_1) is smaller than that of PC II (a_2). As the lattice constants of PCs I and II vary, the transmission frequency range of the line defect also varies [Fig. 13(d)]. This variation ensures that light with a frequency slightly above the mode edge of PC II becomes a propagation mode in the line defect in PC II and becomes an evanescent mode in PC I. When the width of the PC II region and the lattice constant difference are set appropriately, a confined mode is formed, which has a cosine-like envelope in the center and an exponentially decaying envelope at the edges, as will be discussed later.

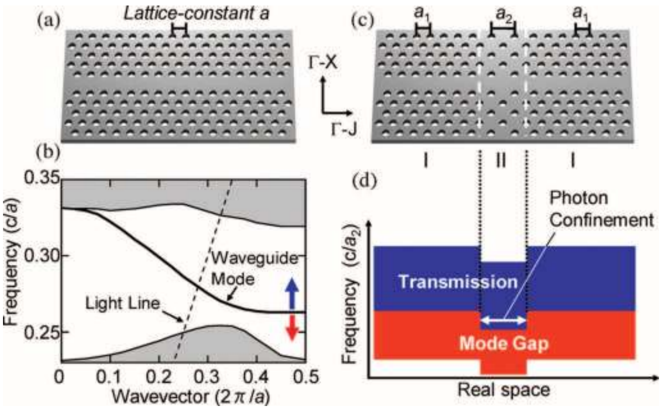

Fig. 13. Basic PC structure and photonic double heterostructure investigated in this paper. (a) 2-D PC slab of triangular-lattice structure with a line-defect waveguide formed by a missing row of air holes in the Γ–J direction. (b) The calculated band structure for the 2-D PC shown in (a). The *blue arrow* indicates the transmission region, in which the propagation of photons is allowed through the waveguide, while the *red arrow* indicates the mode-gap region in which the propagation is inhibited. (c) Photonic double heterostructures, constructed by connecting the basic PC structures I and II. PC I has a triangular-lattice structure with a lattice constant of a_1. PC II has a deformed triangular-lattice structure with a face-centered rectangular lattice of constant $a_2(>a_1)$ in the waveguide direction; it retains the same constant as PC I in the orthogonal direction in order to satisfy the lattice-matching conditions. (d) Schematic of the band diagram along the waveguide direction. Photons of a specific energy can exist only in the waveguide of PC II.

The most important feature of the photonic double-heterostructure nanocavity is that the evanescent behavior of the light in the PC I region is determined by the mode-gap effect in the waveguide, not by the PBG effect [2], [18], [23]. The cavity mode can be determined from the connection of the propagating mode in the PC II region and the evanescent mode in the PC I region. In this cavity, the frequency of the fundamental mode is slightly above the mode edge, of which the wavevector is near the Brillouin zone edge $(k_x = \pi/a)$. According to the Bloch theorem, the propagating mode in the PC II region can be expressed as

$$u(x,y,z)\exp\left(j\frac{\pi}{a}x\right)\exp\left(j\Delta k_x x\right) \tag{3}$$

where $u(x,y,z)$ is a Bloch function with a periodicity of a in the x direction, Δk_x is the difference of the propagation constant from the Brillouin zone edge, and $u(x,y,z)\exp(j\pi x/a)$ is a function with a periodicity of $2a$ in the x direction, which

京都大学 KYOTO UNIVERSITY
A Self-archived copy in
Kyoto University Research Information Repository
https://repository.kulib.kyoto-u.ac.jp
京都大学学術情報リポジトリ KURENAI 紅 Kyoto University Research Information Repository

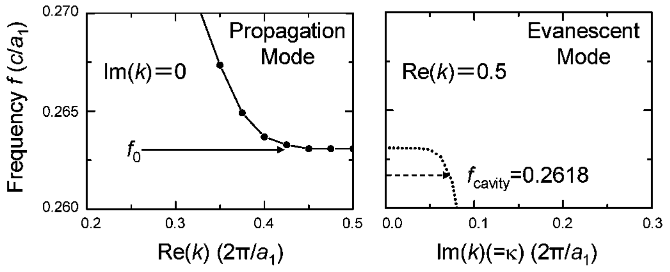

(a) (b)

Fig. 14. (a) Real part of the actual dispersion relation in the PC waveguide I ($a_1 = 410$ nm) [Fig. 13(c)] calculated by a 3-D FDTD. (b) Imaginary part of the wavevector (κ) obtained by Taylor expansion of the dispersion curve near the mode edge (f_0) in (a). The complex wavevector is expressed as $\pi/a_1 + j\kappa$.

corresponds to the fundamental sinusoidal function discussed in Sections II and III. The last part is a slowly varying function that corresponds to the envelope function.

The evanescent mode in the PC I region can be expressed as

$$u'(x, y, z)\exp\left(j\frac{\pi}{a}x\right)\exp(-\kappa x) \tag{4}$$

where u' is a Bloch function with a periodicity of a in the x direction, $u'(x, y, z)\exp(j\pi x/a)$ corresponds to the fundamental sinusoidal function, and $\exp(-\kappa x)$ corresponds to the outer part of the envelope function. Fig. 14 shows the relationship between the frequency and κ in the mode gap, which was obtained by Taylor expansion of the dispersion curve near the mode edge [18]. The cavity frequency was determined so as to fulfill the continuity condition between the propagating modes in PC II and the evanescent modes in PC I at the boundary (or heterointerface). Since a Gaussian function consists of a cosine-like shape in the center region and an overexponential decaying shape at the outer regions, an envelope function formed by $\exp(j\Delta k_x x)$ and $\exp(-\kappa x)$ may be similar to a Gaussian function. It is important to note that κ is spatially constant in the PC I region, so decay of the envelope can be controlled with spatial uniformity. This feature is different from the air-hole shift approach, in which the decay of the envelope around the shifted air holes is changed in a complex way. Since the dependence of κ on the lattice constant difference was known [Fig. 14(b)], we could determine the structural parameters needed to make the envelope function similar to a Gaussian function. Furthermore, we could extend the double heterostructure to a multistep heterostructure, where the outer part of the envelope function is divided into multiple parts, each of which have appropriate values of κ chosen to approximate the Gaussian function more rigorously.

Fig. 15(a) and (b) shows the calculated electric-field distribution of the photonic double-heterostructure cavity and its profile along the waveguide direction, respectively. In Fig. 15(b), the solid-black- and broken-red lines indicate the calculated electric-field distribution and an ideal Gaussian profile, respectively. For the calculation, we used a 3-D FDTD method, assuming lattice constants for PCs I and II of $a_1 = 410$ nm and $a_2 = 420$ nm, respectively, and a slab thickness of $T = 0.6a_2$. The electric-field profile of the photonic double-heterostructure cavity was very close to the ideal Gaussian curve. The Gaussian-like envelope in the photonic double-heterostructure cavity was consistent with the theoretically calculated Q-factors of 2000 000. The modal volume of the photonic double-heterostructure cavity was $\sim 1.2(\lambda_0/n)^3$.

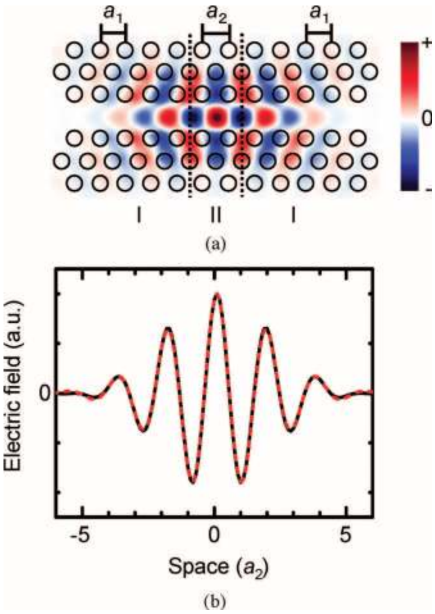

Fig. 15. Calculated results that illustrate the effect of a photonic double heterostructure. (a) Electric-field distribution in the photonic double heterostructure cavity, and (b) its profile along the waveguide direction. A 3-D FDTD method was used for this calculation. The *solid-black-* and *broken-red lines* in (b) indicate the calculated results and the ideal Gaussian profile, respectively.

It should be pointed out that the increase in the modal volume is modest even though the difference between PC I and PC II is small. This is due to the unusual dispersion of the waveguide mode, shown in Fig. 14. As can be seen in Fig. 14(b), the dispersion curve behaves like a step function near the mode edge (f_0), and the imaginary part of the wavevector (κ) takes a relatively large value even though the frequency is close to the mode edge. Therefore, the penetration length of light from PC II into PC I, which can be expressed as $1/2\kappa$, is small, even though the lattice-constant difference between PC I and PC II is small and the cavity resonant frequency is close to the mode edge in PC-I (online supplemental information in [18]).

In light of these theoretical calculations, a photonic double-heterostructure cavity was fabricated by the same method as described in Section III. A plan-view SEM image of the fabricated sample is shown in Fig. 16(a); note that the lattice constant difference is too small to be distinguished by the naked eye. Another waveguide (the input waveguide) was formed parallel to that of the double heterostructure in order to inject photons into the cavity, as shown in Fig. 16(a). For this purpose, the input waveguide was $0.1a_1$ wider [20] than that of the double-heterostructure waveguide.

The cavity Q factor was estimated by the same method as described in Section III. The inset in Fig. 16(b) shows the near-field image observed using an infrared camera, when photons were trapped by the cavity. The trapped light spectrum is shown

京都大学 KYOTO UNIVERSITY
A Self-archived copy in
Kyoto University Research Information Repository
https://repository.kulib.kyoto-u.ac.jp
京都大学学術情報リポジトリ KURENAI 紅 Kyoto University Research Information Repository

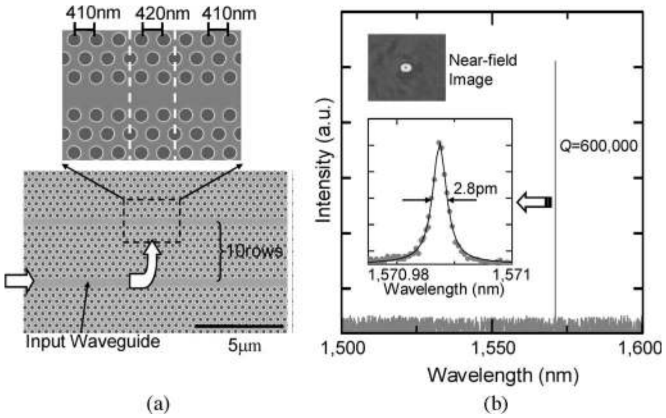

Fig. 16. Experimental results of a double-heterostructure cavity. (a) SEM image of the fabricated photonic double-heterostructure cavity. (b) Resonant spectrum of the cavity over a wide range of wavelengths. The insets show the near-field image observed using an infrared camera and the detailed spectrum at the resonance, respectively. Extremely narrow line widths of 2.8 pm, corresponding to a Q factor of 600 000, were obtained.

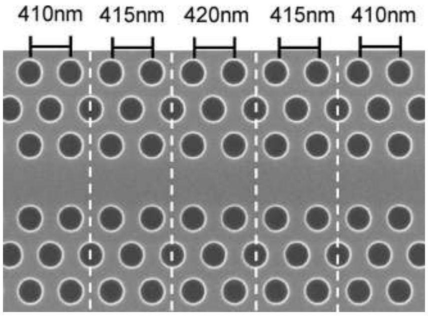

Fig. 17. SEM image of the multistep heterostructure PC cavity designed to have a Q factor of 16 000 000.

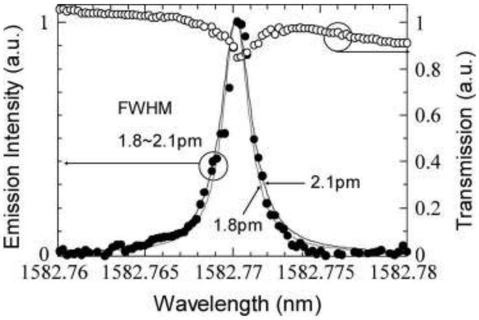

Fig. 18. Measured cavity characteristics of the multistep heterostructure photonic crystal cavity (Fig. 17): Emission spectrum of the cavity (*filled circles*), fitted by Lorentzian functions with FWHM values of 1.8 pm (*red line*) and 2.1 pm (*blue line*); transmittance spectrum of the excitation waveguide (*open circles*).

in Fig. 16(b). An extremely narrow line width of 2.8 pm was obtained. The intrinsic Q factor was estimated to be 600 000, taking into account the effect of coupling between the cavity and the input waveguide. This Q factor is six times larger than the best air-hole-modified cavity, shown in Fig. 12, which indicates that the double heterostructure approach is a more powerful way to tailor the electric field envelope of a cavity mode compared to the air-hole-shifting approach. It is more powerful because the decay constant of the envelope is spatially uniform and is straightforwardly determined by the lattice-constant difference, as discussed earlier.

The key to obtaining cavities with high Q factors is the control of the envelope function, especially the decay behavior of the envelope function in the evanescent region. We utilized a varying lattice constant along the waveguide to control κ, but there are other methods to obtain the same effect. For example, the variation of the waveguide width or variation of the air-hole diameter along the waveguide are also considered capable of tuning the decay of the envelope function, however, the result would be the same. Furthermore, it is very clear that the envelope function can be controlled more flexibly by introducing multistep heterostructures. The lattice constant of a step is determined as a function of the decay constant required for that step to approximate the Gaussian function. An example of a multistep heterostructure cavity, in this case with three steps, is shown in Fig. 17. The lattice constants of the central, the intermediate, and the outer regions were 420, 415, and 410 nm, respectively. The calculated Q factor and the volume of the cavity were $\sim 16\,000\,000$, and $1.23(\lambda_0/n)^3$, respectively. (A cavity with a theoretical Q factor of 20 000 000 has also been designed by changing the air-hole size slightly [18]. The Q factor of 16 000 000 is that calculated for the air-hole size measured in the fabricated cavity.)

The measured emission spectrum of the cavity is plotted in Fig. 18 (filled circles); a sharp resonant peak with a width of the order of a few picometers was seen. The solid lines in Fig. 18 are the Lorentzian fits to the spectrum with FWHM values of 1.8 pm (red) and 2.1 pm (blue).[1] The experimental Q factor of this three-step cavity, evaluated from the values of the FWHM and the waveguide transmittance, was 820 000–950 000. Further increases in the theoretical Q factor are possible by extending the number of steps in the heterostructures to control the envelope function more rigorously. However, the theoretical Q factor seems to have a minor role in determining the experimental Q factors of the latest cavities, as will be discussed in Section V. Since the resonant spectra of high-Q nanocavities are approaching the resolution limits of conventional wavelength meters as described earlier,[1] it is necessary to check the values of Q factors from another type of experiments based on a different principle. Q factor is a measure of cavity loss and is proportional to the lifetime of photons in the cavity (τ). The

---

[1] We believe that it is necessary to reveal the measurement method in detail since the FWHM of the spectrum is of the order of picometers, almost at the limit of resolution. An external cavity, tunable wavelength, semiconductor laser was used (SANTEC, TSL-210). The emission wavelength was changed by controlling the cavity length with a piezo actuator. The width of the laser line was <1 MHz ($\sim$ 8 fm at 1570 nm). Each time the emission wavelength was altered, it was measured using a wavelength meter (Agilent 86122-A-opt-002: with a high-precision option). The differential accuracy of the wavelength meter was ± 0.15 pm. The best Lorentzian fit to the resonant spectrum had a FWHM value of 1.95 pm. We evaluated the range of FWHM value as 1.8–2.1 pm by adding an error value of ± 0.15 pm to the best-fit value. (In addition to the accuracy of the measurement system, there is a problem of temperature fluctuation since temperature dependence of the cavity resonant wavelength is as large as 80 pm/K [31]. This might widen the evaluation range of the FWHM further, namely, the FWHM value might be smaller than 1.8 pm or larger than 2.1 pm.

京都大学 KYOTO UNIVERSITY
A Self-archived copy in
Kyoto University Research Information Repository
https://repository.kulib.kyoto-u.ac.jp
京都大学学術情報リポジトリ KURENAI 紅 Kyoto University Research Information Repository

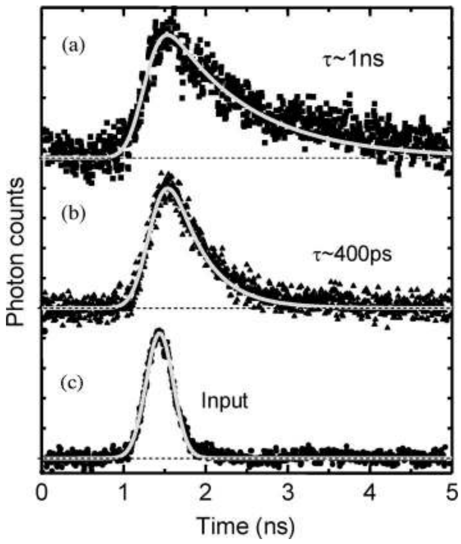

Fig. 19. Results of time-resolved measurement of light emission from cavities. (a) Light emitted from the cavity having a line width of 1.8–2.1 pm (Fig. 18). *Solid line* is a fitting result that assumes the photon lifetime of ~ 1 ns. (b) The evolution of the light emitted from a cavity having a line width of ~ 4.5 pm. *Solid line* is a fitting result that assumes the photon lifetime of ~ 400 ps. (c) The input light pulse. *Solid line* is the fitting result that assumes a Gaussian shape having FWHM of 360 ps.

relationship between them is expressed as $Q = \omega\tau$. Therefore, we can evaluate the Q factors by measuring the time-domain responses of the cavities [24]. Very recently, we have succeeded in measuring the photon lifetime in the high-Q nanocavities. The samples measured were the cavity shown in Fig. 17, which has a line width of 1.8–2.1 pm, and the same-type cavity which has a line width of 4.5 pm. Light emitted from the tunable continuous wave semiconductor laser was modulated by an external electro-optical modulator, and light pulses whose widths were about 300 ps were produced. The light pulses excited the cavities where the center wavelengths were set at the resonance wavelengths, and a photomultiplier tube detected the light emitted from the cavities. The time-resolved signals were obtained by time-correlated single-photon counting method. Time resolution of the measurement system was about 300 ps. The measurement results are shown in Fig. 19. It is seen that the light emitted from the cavities have decaying tails in the later time side, and the decay of the tail is longer for the sample with narrower line width. Numerical fitting of the data were carried out by convoluting the input light pulse shape [Fig. 19(c)] and decay function of $\exp(-t/\tau)$. The results are shown by the solid lines in Fig. 19, where the best fitting results were obtained for $\tau = 1$ ns and ~ 400 ps for the cavities with line widths of 1.8–2.1 pm and ~ 4.5 pm, respectively. The obtained lifetimes of ~ 1 ns and ~ 400 ps correspond to Q factors of about 1.2 and 0.5 million, respectively. The Q factors of the cavities obtained from the time-domain measurement are slightly larger than that obtained from the wavelength-domain measurement. However, the orders of both results are the same, which ensures the validity of the measured Q factors.

V. DISCUSSION ON THE DIFFERENCE BETWEEN EXPERIMENTAL AND THEORETICAL Q FACTORS

Although very high-Q nanocavities were achieved by using double- and multistep heterostructures, the experimental (Q_{exp}) factors obtained (600 000–950 000) were found to be smaller than the theoretical Q factors determined by the cavity design $Q_{\text{design}})$, which were as high as 2 000 000–16 000 000. This mismatch can be explained by introducing an additional Q factor due to imperfections of the fabricated cavity $(Q_{\text{imperfect}})$, such as roughness and contamination. The relationship between these three Q factors is given by

$$\frac{1}{Q_{\text{exp}}} = \frac{1}{Q_{\text{design}}} + \frac{1}{Q_{\text{imperfect}}}. \qquad (5)$$

$Q_{\text{imperfect}}$ was evaluated to be 850 000, and 860 000–1 010 000 for the double- and multistep heterostructure cavities, respectively, indicating that the loss due to imperfections $(1/Q_{\text{imperfect}} = 1/850\,000\text{–}1/1010\,000)$ was larger than the loss determined by design $(1/Q_{\text{design}} = 1/2000000\text{–}1/16000000)$. This means that Q_{exp} was determined by $1/Q_{\text{imperfect}}$ and not by $1/Q_{\text{design}}$. The fact clearly indicates that Q_{exp} will saturate at the level of $Q_{\text{imperfect}}$ despite further increases in Q_{design}. We, therefore, conclude that the key to further increasing the experimental Q factor is to reduce the losses due to imperfections.

As a first step toward this aim, the details of the losses due to imperfections were analyzed. The origins of such losses were categorized as follows:

A) imperfections of the cavity shape;
  A1) surface roughness of the Si slab;
  A2) surface roughness of the inner walls of the air holes;
  A3) variation in the radii of the air holes;
  A4) variation in the positions of the air holes;
  A5) tilt of the inner walls of the air holes;
B) imperfections of the cavity material;
  B1) optical absorption by residual free carriers in the Si slab;
  B2) optical absorption by material, such as water [26], adsorbed [27] to the surfaces of the cavity.

The losses due to each of the previous factors were quantitatively evaluated [28] for the three-step heterostructure cavity. Here, we present the results without showing the evaluation methods due to space limitations. Table I contains the measured quantities on which the calculations were based, and the calculated loss Q factors for each of the seven categories (denoted by A1–A5, B1, and B2).

The inverse of the total theoretical additional loss Q factor $(1/Q_{\text{imperfect}})$ was obtained by summing the inverses of all the calculated Q factors in Table I, giving $Q_{\text{imperfect}} = 900000$. This theoretical value is of the same order as the experimental value, indicating that the results in Table I can be regarded as a measure of the real situation, despite the assumptions used. The dominant losses were associated with the tilt of the inner walls of the air holes $(Q \sim 3\,000\,000$ for a tilt of $3')$, the variation in the radii of the air holes $(Q \sim 3\,000\,000)$, the absorption by the surface water $(Q \sim 4\,000\,000)$, and the surface roughness of the inner walls of the air holes $(Q \sim 5\,500\,000$ for radiation to free

京都大学 KYOTO UNIVERSITY
A Self-archived copy in
Kyoto University Research Information Repository
https://repository.kulib.kyoto-u.ac.jp
京都大学学術情報リポジトリ KURENAI 紅 Kyoto University Research Information Repository

TABLE I
SUMMARY OF THE ORIGINS, MEASURED QUANTITIES, AND CALCULATED Q FACTORS FOR EACH LOSS

Origin	**Quantity**	**Source**	**Calculated Q factor ($\times 10^6$)**		
			Free-space modes	TM-like slab modes	Absorption
A1: Surface roughness of air-hole walls	Lc = ~9 nm σ = ~2 nm	SEM	8	24	—
A2: Surface roughness of slab	Lc = ~9 nm σ = 0.1-0.2 nm	AFM	3,400	2,000	—
A3: Variation in air-hole positions	σ < 1 nm [a]	SEM	17	—	—
A4: Variation in air-hole radii	σ < 1 nm [a]	SEM	3	—	—
A5: Tilt of air-hole walls	< 3°	SEM	—	3 (for 3°)	—
B1: Residual free carriers	$n_c = 10^{15}$ cm^{3} $\rho = 11.5\ \Omega$cm	Substrate specification	—	—	600
B2: Adsorbed water	$\alpha = \sim 10$ cm^{-1}	[25]	—	—	4 [b]

[a] Below measurement limit

[b] Assuming adsorption of 2 atomic layers at the surface of the slab and air-hole walls

Lc: Correlation length, σ: Standard deviation, n_c: Carrier density , ρ: Resistivity, α: Absorption coefficient.

space and transverse magnetic-like slab modes [28], [29]). The tilt and surface roughness of the inner walls of air holes and the variation in air-hole radii are likely to be decreased by reviewing the fabrication processes, e.g., dry etching and electron-beam lithography. The extent of absorption by the surface water ($Q \sim 4\,000\,000$) is also large, but it is poorly understood and needs to be investigated further: measurements *in vacuo* may clarify the extent of the problem. Another surface absorption mechanism such as absorption by the surface states [30] might also have some contribution.

VI. CONCLUSION

We have investigated the confinement mechanism of point-defect cavities in 2-D PC slabs, and have established an important design concept for high-Q nanocavities, namely that the envelope function should be gently varying but remain spatially localized (like a Gaussian function). On the basis of this concept, we have proposed a method of shifting air-hole positions to obtain the desirable envelope function. Using this method, we have designed a cavity with a theoretical Q factor of 200 000 and a cavity volume of $0.71(\lambda_0/n)^3$ and succeeded in experimentally demonstrating a high-Q factor of 100 000. We have further proposed an improved method of tuning the envelope function, using multistep heterostructures, and have designed and fabricated a cavity with a theoretical Q factor of 16 000 000 and a cavity volume of $1.23(\lambda_0/n)^3$. The experimental Q factor of this cavity was almost 1 million, which indicates the power of the multistep heterostructure method. The difference between the theoretical and the experimental Q factors is discussed from the viewpoint of the effect of imperfections in the fabricated structures. The important imperfections of the fabricated structures have been categorized, and the associated losses have been quantified for a multistep heterostructure cavity. It has been shown that the dominant sources of loss are the tilt and roughness of the inner walls of the air holes, variation in air-hole radii, and optical absorption by material (water) adsorbed on the cavity surfaces. We believe that experimental Q factors of the order of a few to several millions will be obtained in the future by solving these problems. We also believe that these results will accelerate developments in various areas, including single-photon emitters for quantum communication and computing, zero-threshold nanolasers, ultrasmall photonic chips, atom trapping, biosensing, and accurate environmental monitors.

REFERENCES

[1] S. Noda, A. Chutinan, and M. Imada, "Trapping and emission of photons by a single defect in a photonic bandgap structure," *Nature*, vol. 407, pp. 608–610, 2000.
[2] B. S. Song, S. Noda, and T. Asano, "Photonic devices based on in-plane heterophotonic crystals," *Science*, vol. 300, p. 1537, 2003.
[3] H. Takano, Y. Akahane, T. Asano, and S. Noda, "In-plane-type channel drop filter in a two-dimensional photonic crystal slab," *Appl. Phys. Lett.*, vol. 84, no. 13, pp. 2226–2228, 2004.
[4] H. Takano, B. S. Song, T. Asano, and S. Noda, "Highly efficient in-plane channel drop filter in a two-dimensional heterophotonic crystal," *Appl. Phys. Lett.*, vol. 86, pp. 241101-1–241101-3, 2005.
[5] M. Lončar, A. Scherer, and Y. Qiu, "Photonic crystal laser sources for chemical detection," *Appl. Phys. Lett.*, vol. 82, no. 26, pp. 4648–4650, 2003.
[6] O. Painter, R. K. Lee, A. Scherer, A. Yariv, J. D. O'Brien, P. D. Dapkus, and I. Kim, "Two-dimensional photonic band-gap defect mode laser," *Science*, vol. 284, pp. 1819–1821, 1999.
[7] P. Michler, A. Kiraz, C. Becher, W. V. Schoenfeld, P. M. Petroff, L. Zhang, E. Hu, and A. Imamoğlu, "A quantum dot single-photon turnstile device," *Science*, vol. 290, pp. 2282–2285, 2000.
[8] M. F. Yanik and S. Fan, "Stopping light all optically," *Phys. Rev. Lett.*, vol. 92, no. 8, pp. 083901-1–083901-4, 2004.
[9] Y. Tanaka, T. Asano, and S. Noda, "Trapping of ultrashort optical pulse into ultra-high-Q photonic nanocavity," presented at the Int. Conf. Quantum Electronics 2005 and the Pacific Rim Conf. Lasers and Electro-Optics 2005, CWE4-3, Toshi Center Kaikan, Tokyo, Japan, Jul. 13, 2005.
[10] S. G. Johnson, S. Fan, A. Mekis, and J. D. Joannopoulos, "Multipole-cancellation mechanism for high-Q cavities in the absence of a complete photonic band gap," *Appl. Phys. Lett.*, vol. 78, no. 22, pp. 3388–3390, 2001.
[11] J. Vučković, M. Lončar, H. Mabuchi, and A. Scherer, "Design of photonic crystal microcavities for cavity QED," *Phys. Rev. E, Stat. Phys. Plasmas Fluids Relat. Interdiscip. Top.*, vol. 65, pp. 016608-1–016608-11, 2001.
[12] J. Vučković, M. Lončar, H. Mabuchi, and A. Scherer, "Optimization of the Q factor in photonic crystal microcavities," *IEEE J. Quantum Electron.*, vol. 38, no. 7, pp. 850–856, Jul. 2002.
[13] K. Srinivasan and O. Painter, "Momentum space design of high-Q photonic crystal optical cavities," *Opt. Exp.*, vol. 10, no. 15, pp. 670–684, 2002.
[14] H. Y. Ryu, M. Notomi, and Y. H. Lee, "High-quality-factor and small-mode-volume hexapole modes in photonic-crystal-slab nanocavities," *Appl. Phys. Lett.*, vol. 83, no. 21, pp. 4294–4296, 2003.
[15] K. Srinivasan, P. E. Barclay, O. Painter, J. Chen, A. Y. Cho, and C. Gmachl, "Experimental demonstration of a high quality factor photonic crystal microcavity," *Appl. Phys. Lett.*, vol. 83, no. 10, pp. 1915–1917, 2003.
[16] Y. Akahane, T. Asano, B. S. Song, and S. Noda, "High-Q photonic nanocavity in a two-dimensional photonic crystal," *Nature*, vol. 425, pp. 944–947, 2003.
[17] ——, "Fine-tuned high-Q photonic-crystal nanocavity," *Opt. Exp.*, vol. 13, pp. 1202–1214, 2005.
[18] B. S. Song, S. Noda, T. Asano, and Y. Akahane, "Ultra-high-Q photonic double-heterostructure nanocavity," *Nat. Mater.*, vol. 4, no. 3, pp. 207–210, 2005.
[19] D. Englund, I. Fushman, and J. Vučković, "General recipe for designing photonic crystal cavities," *Opt. Exp.*, vol. 13, no. 16, pp. 5961–5975, 2005.
[20] S. Ogawa, M. Imada, S. Yoshimoto, M. Okano, and S. Noda, "Control of light emission by 3D photonic crystals," *Science*, vol. 10. 1126/science. 1097968, 2004.

京都大学 KYOTO UNIVERSITY
A Self-archived copy in
Kyoto University Research Information Repository
https://repository.kulib.kyoto-u.ac.jp
京都大学学術情報リポジトリ KURENAI 紅 Kyoto University Research Information Repository

[21] Y. Akahane, M. Mochizuki, T. Asano, Y. Tanaka, and S. Noda, "Design of a channel drop filter by using a donor-type cavity with high-quality factor in a two-dimensional photonic crystal slab," *Appl. Phys. Lett.*, vol. 82, no. 9, pp. 1341–1343, 2003.

[22] Y. Akahane, T. Asano, B.-S. Song, and S. Noda, "Investigation of high-Q channel drop filters using donor-type defects in two-dimensional photonic crystal slabs," *Appl. Phys. Lett.*, vol. 83, no. 8, pp. 1512–1514, 2003.

[23] B. S. Song, T. Asano, Y. Akahane, and S. Noda, "Role of interfaces in heterophotonic crystals for manipulation of photons," *Phys. Rev. B, Condens. Matter*, vol. 71, pp. 195101-1–195101-5, 2005.

[24] T. Asano, W. Kunishi, B.-S. Song, and S. Noda, "Time-domain response of point-defect cavities in two-dimensional photonic crystal slabs using picosecond light pulse," *Appl. Phys. Lett.*, vol. 88, no. 151102, pp. 1–3, 2006.

[25] M. Chaplin. (2005, May12). Water structure and behavior [Online]. Available: http://www.lsbu.ac.uk/water/

[26] D. Liu, G. Ma, M. Xu, and H.C. Allen, "Adsorption of ethylene glycol vapor on r-Al_2 O_3 (0001) and amorphous SiO_2 surfaces: Observation of molecular orientation and surface hydroxyl groups as sorption sites," *Environ. Sci. Technol.*, vol. 39, pp. 206–212, 2005.

[27] T. Asano, B. S. Song, and S. Noda, "Analysis of the experimental Q factors ($\sim$ 1 million) of photonic crystal nanocavities," *Opt. Exp.*, vol. 14, pp. 1996–2002, 2006.

[28] Y. Tanaka, T. Asano, Y. Akahane, B. S. Song, and S. Noda, "Theoretical investigation of propagation loss of a line defect waveguide in a two-dimensional photonic crystal slab with tapered air holes," *Appl. Phys. Lett.*, vol. 82, pp. 1661–1663, 2003.

[29] Y. Tanaka, T. Asano, R. Hatsuta, and S. Noda, "Investigation of point-defect cavity formed in two-dimensional photonic crystal slab with one-sided dielectric cladding," *Appl. Phys. Lett.*, vol. 88, p. 011112, 2006.

[30] M. Borselli, T. J. Johnson, and O. Painter, "Beyond the Rayleigh scattering limit in high-Q silicon microdisks: Theory and experiment," *Opt. Exp.*, vol. 13, pp. 1515–1530, 2005.

[31] T. Asano, W. Kunishi, M. Nakamura, B. S. Song, and S. Noda, "Dynamic wavelength tuning of channel-drop device in two-dimensional photonic crystal slab," *Electron. Lett.*, vol. 41, pp. 37–38, 2005.

Takashi Asano received the B.S., M.S., and Ph.D. degrees from Kyoto University, Kyoto, Japan, in 1992, 1994, and 1997, respectively, all in electronics.

From 1996 to 1998, he was a Research Fellow with the Japan Society for the Promotion of Science at Kyoto University. From 1999 to 2000, he was a Postdoctoral Fellow at the Kyoto University Venture Business Laboratory, Kyoto. He joined Kyoto University, in 2000, and is currently a Lecturer in the Department of Electronic Science and Engineering. His research has been concerned with intersubband transitions in quantum wells, ultrafast phenomena in semiconductors, and 2-D photonic crystals. His current research interests include defect engineering and light–matter interaction in semiconductor-based 2-D photonic crystals.

Dr. Asano is a member of the Japan Society of Applied Physics.

Bong-Shik Song received the B.S. and the M.S. degrees from Inha University, Incheon, Korea, in 1999, and 2001, respectively, both in electrical engineering. He received the Ph.D. degree in electronics from Kyoto University, Kyoto, Japan, in 2004.

From 2004 to 2006, he was a Research Fellow with Japan Science and Technology Agency at Kyoto University. In March 2006, he joined Sungkyunkwan University, Suwon, Korea, and is currently an Assistant Professor with the School of Information and Communication Engineering. His current research interests include 2-D photonic crystals and their application to novel functional photonic devices.

Dr. Song is a member of the Optical Society of America.

Yoshihiro Akahane received the B.S. and the M.S. degrees from Kyoto University, Kyoto, Japan, in 1992 and 1994, respectively, both in chemistry. He received the Ph.D. degree in electronics from Kyoto University, in 2005.

From 1994 to 2001, he was with Sumitomo Electric Industries Ltd., Osaka, Japan. From 2001 to 2005, he was a Research Fellow at Kyoto University for their collaboration research with Sumitomo Electric. He is currently with Sumitomo Electric. His research has been concerned with 2-D photonic crystals and their application to novel functional photonic devices. His current research interests include new materials and their application to photonic devices.

Dr. Akahane is a member of the Japan Society of Applied Physics.

Susumu Noda (M'92) received the B.S., M.S., and Ph.D. degrees from Kyoto University, Kyoto, Japan, in 1982, 1984, and 1991, respectively, all in electronics. He received an Honorary Doctorate degree from Ghent University, Ghent, Belgium, in 2006.

From 1984 to 1988, he was with Mitsubishi Electric Corporation, Hyogo, Japan, and was engaged in research on optoelectronic devices including AlGaAs/GaAs distributed feedback (DFB) lasers and multiple quantum well DFB lasers. He joined Kyoto University, in 1988, and is currently a Professor in the Department of Electronic Science and Engineering. His research has been concerned with ultrafast phenomena using intersubband transitions in quantum wells, growth and characterization of InAs self-assembled quantum dots on GaAs substrate, and semiconductor-based 3-D and 2-D photonic crystals. He is an author of more than 200 scientific papers published in international journals. He has organized numerous symposia on photonic nanaostructures. His current research interests include quantum optoelectronics including photonic and/or quantum nanostructures.

Dr. Noda is a member of the Institute of Electrical, Information and Communication Engineers, Japan and the Japan Society of Applied Physics (JSAP). He has served as an IEEE LEOS Distinguished Lecturer from 2003 to 2005. He was the recipient of various awards including the IBM Science Award, 2000, Osaka Science Award, 2004, and the JSAP Achievement Award for Quantum Electronics, 2005.